MOLECULAR PHYSICS, 2003, VOL. 101, NO. 7, 1047–1056

Taylor & Francis
Taylor & Francis Group

Luminescence spectroscopy of high-energy $4f^{11}$ levels of Er^{3+} in fluorides

R. T. WEGH[1]†, E. V. D. VAN LOEF[1], G. W. BURDICK[2] and A. MEIJERINK[1]*

[1]Debye Institute, Utrecht University, PO Box 80 000, 3508 TA Utrecht, The Netherlands

[2]Department of Physics, Andrews University, Berrien Springs, MI 49104, USA

The $4f^{11}$ energy levels of Er^{3+} in $LiYF_4$ in the spectral region 39 000–65 000 cm^{-1} have been studied. The agreement between experimental energy levels, obtained from luminescence excitation spectra, and calculated energy levels is good. Luminescence originating from high-lying energy levels has been investigated. Emission from the states $^4D_{1/2}$ (~47 200 cm^{-1}), $^2F(2)_{7/2}$ (~54 700 cm^{-1}) and $^2F(2)_{5/2}$ (~63 300 cm^{-1}) is observed. $^2F(2)_{5/2}$ emission occurs for Er^{3+} in LaF_3, where the $^2F(2)_{5/2}$ level is situated just below the lowest $4f^{10}5d$ state, but also for Er^{3+} in $LiYF_4$, where it lies in between the two lowest $4f^{10}5d$ states.

1. Introduction

The need for luminescent materials for excitation in the vacuum ultraviolet spectral region (VUV; $E > 50\,000\,cm^{-1}$, $\lambda < 200\,nm$) has triggered an increase in research on the VUV spectroscopy of lanthanides. These materials (VUV phosphors) are required for application in mercury-free fluorescent lamps and in plasma display panels [1]. In these devices the VUV radiation generated by a noble gas discharge (e.g. Xe) has to be converted into visible light. In theory, the high energy of VUV photons is sufficient to generate two visible photons for each VUV photon absorbed by a phosphor. In other words, it is theoretically possible to obtain visible quantum efficiencies higher than 100%, which is called quantum cutting. In contrast, the quantum efficiencies of (UV) phosphors used in mercury discharge fluorescent tubes cannot exceed 100% due to the lower energy of the exciting photons. The use of VUV phosphors with quantum efficiencies above 100% can compensate for the lower number of photons generated per watt by the noble gas discharge relative to the mercury discharge.

Because of their sharp-line emissions, trivalent lanthanide ions are optical centres for which quantum cutting, or photon-cascade emission, can possibly be obtained. Indeed, quantum cutting has been demonstrated for Pr^{3+}-doped fluorides [2, 3] and studied theoretically for a number of lanthanides using Judd–Ofelt calculations [4, 5]. Unfortunately, it was concluded that although quantum cutting can occur for certain lanthanides, the quantum efficiency in the useful visible spectral region will not be higher than 100%. However, this conclusion was based on the $4f^n$ energy levels of lanthanides up to 50 000 cm^{-1}, since (nearly) nothing was known on $4f^n$ levels in the VUV spectral region. An overview of the levels of all lanthanides in the IR, visible and UV was already reported more than 30 years ago [6]. Since then many research groups have worked on the improvement of measurements and calculations of these $4f^n$ levels [7]. Reports on $4f^n$ energy levels above 50 000 cm^{-1} are scarce [8–11], mainly because it is experimentally difficult to measure weak (parity-forbidden) $4f^n \rightarrow 4f^n$ transitions in the VUV.

In order to investigate if efficient visible quantum cutting is possible, we have explored the spectroscopy of high energy levels for all trivalent lanthanides of interest by the following method. First, the energy levels in the VUV region are elucidated, experimentally by VUV spectroscopy and theoretically by energy level calculations. Next, it is investigated if emission from a high level takes place. If this is the case, the possibility of sequential emission of two visible photons with this high level as a starting level is studied. In previous papers we have reported the results for Gd^{3+} ($4f^7$) [12] and Ho^{3+} ($4f^{10}$) [13]. It was shown that quantum cutting occurs, albeit not efficiently in the visible. For Gd^{3+} it was shown that the visible quantum efficiency

* Author for correspondence. e-mail: A.Meijerink@phys.uu.nl

† Present address: Philips Research Laboratories, Prof. Holstlaan 4, 5656 AA Eindhoven, The Netherlands.

Molecular Physics ISSN 0026–8976 print/ISSN 1362–3028 online © 2003 Taylor & Francis Ltd
http://www.tandf.co.uk/journals
DOI: 10.1080/0026897021000046906

can be enhanced by a two-step energy transfer to Eu^{3+} [14]. Here the spectroscopy of the high levels of Er^{3+} ($4f^{11}$) is presented. Er^{3+} is a promising candidate for quantum cutting because of its relatively simple $4f^{11}$ energy level scheme and the relatively large gaps between different levels. Energy gaps are important because only when the gap to the next lower level is large enough, does the emission from a certain energy level become more probable than multiphonon relaxation [15]. An additional advantage of Er^{3+} is the high energy of the $4f^{10}5d$ configuration, the lowest opposite-parity state, making the observation of the weak $4f^{11} \rightarrow 4f^{11}$ transitions at high energies possible. Here we report the luminescence of Er^{3+} incorporated in fluorides, e.g. $LiYF_4$ and LaF_3, because in these host lattices the phonon energies are small and the $4f^{10}5d$ states are at the highest possible energies. The $4f^{11}$ energy level diagram of Er^{3+} in fluoride hosts is given in figure 1. Every $^{2S+1}L_J$ multiplet, which is denoted by one horizontal line in figure 1, is split into several Stark levels by the crystal field. For a number of multiplets the $^{2S+1}L_J$ term symbol is given, but not for all. The VUV energy levels are also present in figure 1, as the approximate positions are known from calculations, but they have never been studied experimentally and theoretically in detail, although some excellent experimental work on *f–f* and *f–d* emission for Er^{3+} $LiYF_4$ was recently reported in [8]. The results of our investigation on this are discussed in section 3.1. In section 3.2 it will be shown that emission from several high $4f^{11}$ levels occurs.

2. Experimental

The Er^{3+}-doped fluoride samples were prepared in a glassy carbon crucible in a nitrogen atmosphere using a high-frequency furnace [12]. Flushing with SF_6 as a reactive agent during heating was used to eliminate oxygen in the samples [16]. Slow cooling from the melt (1 to 5 days) resulted in oxygen-free, transparent single crystals for Er^{3+} in $LiYF_4$ and LaF_3, which were polished before the spectroscopic measurements. For YF_3:Er^{3+} a polycrystalline powder was obtained after grinding, which was checked for phase purity by X-ray powder diffraction.

The high-resolution excitation spectra needed to elucidate the high energy levels were measured with synchrotron radiation as the excitation source at the HIGITI set-up of HASYLAB at DESY, Hamburg (Germany). VUV–UV emission and luminescence decay measurements were also performed with this experimental set-up. Experiments could be done at cryogenic temperatures by means of a cold finger liquid helium cryostat. The excitation spectra were corrected for the intensity of the synchrotron radiation and the transmission of the monochromator. The UV–visible emission spectra upon excitation in the VUV were recorded on a modified Spex 1680 spectrofluorometer at room temperature. The spectra were corrected for

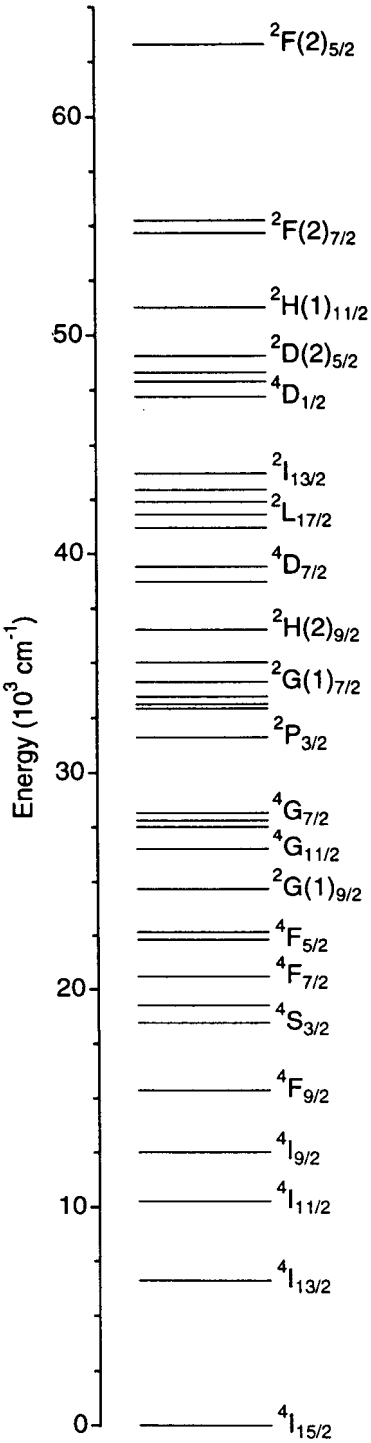

Figure 1. Energy level diagram in the range 0–65 000 cm^{-1} for Er^{3+}.

the transmission of the emission monochromator and the detector response. Both set-ups are described extensively in [12], and details on the time-resolved measurements are given in [17].

3. Results and discussion

3.1. *Elucidation of high-energy levels*

For our spectroscopic investigation of the high-energy $4f^{11}$ levels of Er^{3+} we have used a $LiYF_4$:Er^{3+} 2% single crystal. The energy levels of Er^{3+} in $LiYF_4$ in the IR and visible spectral region have been studied since 1969 [18]. Only recently measurements and simulations of the levels in Er^{3+}-doped $LiYF_4$ up to 44 000 cm^{-1} were reported [19]. Therefore, first our results on the energy levels in the region 39 000–44 000 cm^{-1} are compared with those from [19] (table 1), and next the previously unobserved higher-energy transitions are discussed (table 2).

In figure 2 two excitation spectra of the $LiYF_4$:Er^{3+} crystal are presented, recorded by detecting all visible emission using a colour filter with a photomultiplier tube (no emission monochromator). The upper spectrum shows all excitation lines to $4f^{11}$ levels in the 39 000–45 000 cm^{-1} range. The transition energies determined from the spectrum are listed in table 1, together with the corresponding experimental energies from [19] and calculated energies obtained by fitting our experimental data.

By comparison with the calculated levels in table 1, each sharp excitation line in figure 2 (*a*) can be assigned a transition to a $^{2S+1}L_J$ multiplet. The broader lines around 237 nm are attributed to vibronic transitions belonging to the zero-phonon $^4I_{15/2} \rightarrow {}^2L_{17/2}$ excitations (relatively strong vibronic lines at about 300 cm^{-1} from the zero-phonon line have been reported for several lanthanides in $LiYF_4$ [20]). Similarly the broadening

Table 1. Experimentally observed and calculated $4f^{11}$ energy levels for $LiYF_4$:Er^{3+} in the range 39 000–45 000 cm^{-1}.

Multiplet	E_{exp}/cm^{-1} this work	E_{exp}/cm^{-1} [19]	E_{exp}/cm^{-1} corrected	E_{calc}/cm^{-1}
$^4D_{7/2}$	39 296	39 340	39 341	39 406
	39 382	39 431	39 427	39 413
	39 513	39 552	39 558	39 519
	39 604	—	39 649	39 619
$^2I_{11/2}$	41 100	41 125	41 145	41 144
	—	41 145	—	41 157
	41 162	41 205	41 207	41 214
	—	—	—	41 217
	41 241	41 285	41 286	41 278
	41 285	41 336	41 330	41 327
$^2L_{17/2}$	41 561	41 598	41 606	41 624
	41 644	—	41 689	41 627
	41 684	41 725	41 729	41 773
	41 721	41 758	41 766	41 775
	—	—	—	41 807
	41 790	41 830	41 835	41 843
	41 857	41 902	41 902	41 895
	—	—	—	41 944
	41 922	41 951	41 967	41 977
$^4D_{3/2}$	42 339	42 375	42 384	42 384
	42 367	42 410	42 412	42 414
$^2D_{3/2}$	42 898	—	42 943	42 951
	—	—	—	42 987
$^2I_{13/2}$	—	—	—	43 510
	43 473	43 526	43 518	43 518
	—	43 640	—	43 619
	43 596	43 649	43 641	43 643
	—	—	—	43 788
	43 750	43 796	43 795	43 792
	43 812	43 886	43 857	43 851

Table 2. Experimentally observed and calculated $4f^{11}$ energy levels for $LiYF_4:Er^{3+}$ in the range 45 000–65 000 cm^{-1}.

Multiplet	E_{exp}/cm^{-1}	E_{exp}/cm^{-1} corrected	E_{calc}/cm^{-1}
$^4D_{1/2}$	~47 200[a]	47 245	47 235
$^2L_{15/2}$	—	—	47 792
	47 783	47 828	47 803
	47 856	47 901	47 911
	—	—	47 933
	47 927	47 972	47 985
	—	—	48 016
	47 992	48 037	48 046
	—	—	48 099
$^2H(1)_{9/2}$	48 158	48 203	48 213
	48 216	48 261	48 247
	—	—	48 295
	48 305	48 350	48 359
	—	—	48 419
$^2D(2)_{5/2}$	49 039	49 084	49 082
	49 063	49 108	49 102
	49 188	49 233	49 260
$^2H(1)_{11/2}$	—	—	51 108
	51 078	51 123	51 109
	51 209	51 254	51 240
	—	—	51 340
	51 327	51 372	51 376
	—	—	51 398
$^2F(2)_{7/2}$	54 696	54 741	54 713
	54 723	54 768	54 764
	54 746	54 791	54 807
	54 780	54 825	54 826
$^2D(2)_{3/2}$	55 310	55 355	55 336
	—	—	55 412
$^2F(2)_{5/2}$	~63 300[a]	63 345	63 369
			63 378
			63 412

[a] These approximate values are determined from emission (see section 3.2).

on the short-wavelength side of the $^4D_{7/2}$ multiplet (252–255 nm) is probably also due to vibronics. In the region 39 000–45 000 cm^{-1} we have observed 22 of the 30 theoretical levels, while in [19] 21 experimental levels are reported. It can be seen in table 1 that the crystal-field splittings of $^{2S+1}L_J$ states are very similar, indicating that the transitions observed by us and by Couto dos Santos *et al.* are the same. Although this is indeed most probable, it is difficult to prove as no spectra are shown in [19]. Thus, in table 1 the levels we measured are listed in such a way that the energy differences with the experimental levels from [19] are as similar as possible, and therefore not necessarily as small as possible. It appears that our experimental energies in this region are systematically some 40–50 cm^{-1} lower than the energies in [19]. This discrepancy is probably caused by an error in the calibration of the excitation monochromator used for our measurements. In order to correct for the calibration error, 45 cm^{-1} was added to all experimental energies (E_{exp} corrected in table 1) and these values were used for the fit. For all levels below 39 000 cm^{-1} the experimental data from [19] were used.

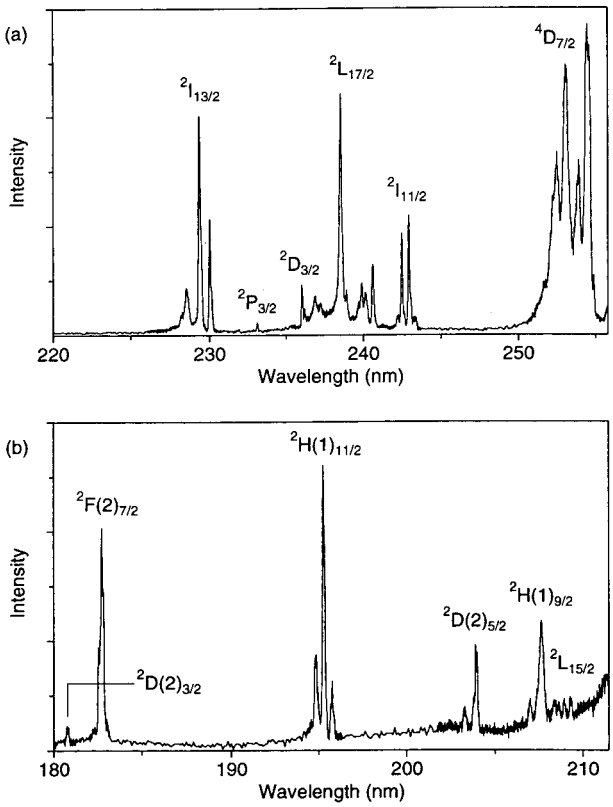

Figure 2. Excitation spectra of $LiYF_4:Er^{3+}$ 2% in the ranges (*a*) 39 000–45 500 cm^{-1} and (*b*) 47 000–55 500 cm^{-1}, both monitoring all visible emission at 9 K.

The spectrum in figure 2 (*b*) is the excitation spectrum measured for $LiYF_4:Er^{3+}$ in the region 47 000–56 000 cm^{-1}, showing a number of sharp lines which can all be assigned to transitions of Er^{3+} $4f^{11}$ multiplets (table 2). In the 45 500–47 000 cm^{-1} region, which is omitted in figure 2, no Er^{3+} $4f^{11}$ excitations are present. The sloping increase on the long-wavelength side of figure 2 (*b*) is attributed to the $4f^8 \rightarrow 4f^7 5d$ excitation on Tb^{3+} [17], which is present as an impurity. In table 2 the positions of the 18 experimentally observed levels and the 29 theoretical levels in the 47 000–56 000 cm^{-1} range are tabulated. The excitation to the single $^4D_{1/2}$ level, which is expected at 212 nm, could not be observed, just as in the earlier work on $LaF_3:Er^{3+}$ by Carnall *et al.* [7, 8]. For the $^2F(2)_{7/2}$ multiplet all four

Stark levels could be resolved by careful measurement, in spite of the small splitting.

For the energy level fit $45\,cm^{-1}$ was added to all experimental energies (E_{exp} corrected in table 2) because of the experimental error mentioned above. The energy level calculation was performed assuming D_{2d} symmetry (which is reasonable although the actual site symmetry is S_4 [19]), and with inclusion of δ-function correlation-crystal-field (CCF) contributions [21]. The parameter values obtained from the fit are given in table 3. The parameters D_0^2 and D_0^4 represent the δ-function CCF contribution [21]. With an overall root-mean-square error of $15.5\,cm^{-1}$ the correspondence between experimental and theoretical levels is good.

It should be noted that the assignment of $^{2S+1}L_J$ terms to the $4f^{11}$ levels of Er^{3+} is not always unambiguous, but varies for different energy level calculations [7, 8, 19]. This is due to the relatively strong mixing of several $^{2S+1}L_J$ terms, often with the same J, which causes for certain levels several terms with a large contribution. It depends on the calculation which term will have the largest weight in these levels. Strong mixing is commonly observed for high-energy $4f^n$ states of lanthanides.

Table 3. Free-ion and crystal-field parameters used for the energy level calculations for $LiYF_4:Er^{3+}$ in tables 1 and 2.

Parameter	Value/cm^{-1}
E_{avg}	35 810
F^2	97 565
F^4	68 445
F^6	55 747
ζ	2 374
α	18.4
β	−583
γ	1 446
T^2	472
T^3	39
T^4	103
T^6	−342
T^7	343
T^8	356
M^0	4.2
P^2	657
B_0^2	308
B_0^4	−523
B_4^4	−953
B_0^6	23
B_4^6	−623
D_0^2	−3.6
D_0^{4a}	3.7
N^b	129
σ^c	15.5

[a] D_4^4/D_0^4 ratio held fixed according to B_4^4/B_0^4 ratio.
[b] Number of experimental energy levels included in the data fit.
[c] Root-mean-square deviation between calculated and observed energy-level data.

The highest level for which an experimental energy was obtained is the $^2F(2)_{5/2}$ state ($\sim 63\,300\,cm^{-1}$), although it could not be observed in excitation. As will be discussed in section 3.2, the experimental values in table 2 for $^2F(2)_{5/2}$ and $^4D_{1/2}$ were determined from emission. Thus, the only multiplets that remain unobserved for Er^{3+} are $^2G(2)_{7/2,9/2}$ and $^2F(1)_{5/2,7/2}$ at energies between 66 000 and $100\,000\,cm^{-1}$.

3.2. *Emission from high-energy levels*

The occurrence of emission from an excited state is in competition with non-radiative decay, and depends on the energy gap to the next lower state and the maximum phonon energy of the lattice. The number of phonons and the phonon energies involved vary for different non-radiative transitions in different systems [15]. For lanthanides in $LiYF_4$, in which the maximum phonon energy is $\sim 560\,cm^{-1}$ [22], as a rule of thumb emission from a $4f^n$ level can compete with multiphonon relaxation if the gap to be bridged is larger than some $2000\,cm^{-1}$. Consequently, for $LiYF_4:Er^{3+}$ there are a number of emitting levels, e.g. $^4F_{9/2}$ at $\sim 15\,300\,cm^{-1}$, $^4S_{3/2}$ at $\sim 18\,400\,cm^{-1}$ and $^2P_{3/2}$ at $\sim 31\,600\,cm^{-1}$. In the presently studied high-energy region, emission from the $^4D_{1/2}$ and $^2F(2)_{7/2}$ levels can be expected to take place.

To investigate if $^4D_{1/2}$ emission occurs, emission spectra (not shown) of the $LiYF_4:Er^{3+}$ crystal were recorded upon excitation into the $^2H(1)_{9/2}$ and $^2H(1)_{11/2}$ states at 207.9 and 195.6 nm respectively. Indeed, in these spectra a number of sharp emission lines are present which are not observed upon excitation into lower Er^{3+} levels. All these lines can be identified as transitions from $^4D_{1/2}$ to lower $4f^{11}$ states. The positions of these emission lines are given in table 4. For $\lambda < 300$ nm the positions were determined from emission spectra recorded at HIGITI , for $\lambda > 300$ nm they follow from spectra from the spectrofluorometer. As can be seen in table 4, the transitions from $^4D_{1/2}$ to all states up to $^4G_{11/2}$ are observed except for the emissions to the $^4I_{15/2}$ ground state and the $^2G(1)_{9/2}$ state. The $^4D_{1/2} \rightarrow {}^4G_{9/2}, {}^2K_{15/2}, {}^4G_{7/2}$ emissions could not be identified because they are obscured by the strong $^4S_{3/2}, {}^2H(2)_{11/2} \rightarrow {}^4I_{15/2}$ emissions around 520 to 550 nm (emission from the $^2H(2)_{11/2}$ state, which lies just above the $^4S_{3/2}$ state, can occur at room temperature due to thermal population). At longer wavelengths no $^4D_{1/2}$ emissions were observed, apparently because

Table 4. Wavelengths of observed emissions from high energy levels of Er^{3+}. The $^4D_{1/2}$ and $^2F(2)_{7/2}$ emissions are for Er^{3+} in $LiYF_4$ and the $^2F(2)_{5/2}$ emissions for Er^{3+} in LaF_3.

	Emitting state		
Final state	$^4D_{1/2}$	$^2F(2)_{7/2}$	$^2F(2)_{5/2}$
$^4I_{15/2}$	—	—	158 nm
$^4I_{13/2}$	245 nm	—	176 nm
$^4I_{11/2}$	270 nm	225 nm	188 nm
$^4I_{9/2}$	287 nm	236 nm	196 nm
$^4F_{9/2}$	315 nm	—	208 nm
$^4S_{3/2}$	347 nm	276 nm	222 nm
$^2H(2)_{11/2}$	356 nm	282 nm	226 nm
$^4F_{7/2}$	375 nm	—	234 nm
$^4F_{5/2}$, $^4F_{3/2}$	[a], 407 nm	—	244 nm
$^2G(1)_{9/2}$	—	333 nm	258 nm
$^4G_{11/2}$	480 nm	354–356 nm	271 nm
$^4G_{9/2}$, $^2K_{15/2}$, $^4G_{7/2}$	[a]	369–276 nm	278–283 nm
$^2P_{3/2}$		433 nm	316 nm
$^2K_{13/2}$, $^2P_{1/2}$, $^4G_{5/2}$		466 nm[a]	329–333 nm
$^2G(1)_{7/2}$		—	341 nm
$^2D(1)_{5/2}$		505 nm	351 nm
$^2H(2)_{9/2}$		[a]	371–375 nm
$^4D_{5/2}$			[a]
$^4D_{7/2}$			—
$^2I_{11/2}$			449–452 nm
$^2L_{17/2}$			[a]
$^4D_{3/2}$			476 nm
$^2P_{3/2}$			490 nm
$^2I_{13/2}$			507 nm

[a] Emission is obscured by other emissions.

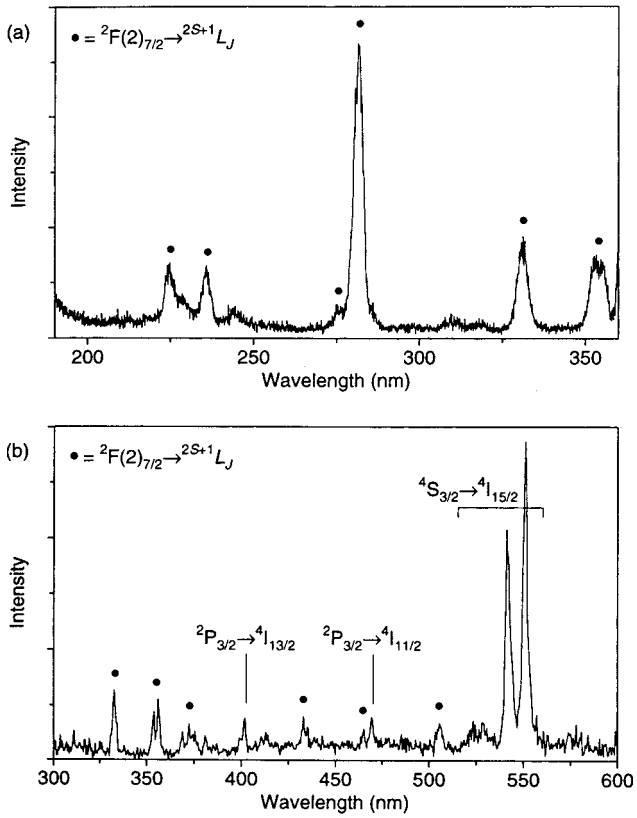

Figure 3. (*a*) UV emission spectrum of $LiYF_4:Er^{3+}$ 2% upon $^4I_{15/2} \rightarrow ^2F(2)_{7/2}$ excitation (182.9 nm) at 7 K. (*b*) UV–visible emission spectrum of $LiYF_4:Er^{3+}$ 2% upon $^4I_{15/2} \rightarrow ^2F(2)_{7/2}$ excitation (182.9 nm) at 300 K. For assignments of the $^2F(2)_{7/2}$ emissions (•) see table 4.

they are too weak (emission spectra were recorded up to 800 nm). The strongest $^4D_{1/2}$ emissions are the emissions to $^4I_{9/2}$, $^4F_{9/2}$ and $^4F_{7/2}$, which are all spin allowed and all lie in the UV.

The observation of $^4D_{1/2}$ emission was reported before for Er^{3+} in YAG and $YAlO_3$ [23]. In these aluminates $^4D_{1/2}$ emission occurs upon excitation in the $4f^{10}5d$ states of Er^{3+}, since the lowest $4f^{10}5d$ state is so close to the $4f^{11}$ levels between 47 000 and 50 000 cm^{-1} that non-radiative decay to $^4D_{1/2}$ takes place. The positions and relative intensities of the $^4D_{1/2}$ emissions in YAG and $YAlO_3$ and in $LiYF_4$ are in good agreement. In the aluminates the emissions are slightly redshifted due to the larger nephelauxetic effect with respect to fluorides.

In figure 3 two emission spectra recorded upon $^2F(2)_{7/2}$ excitation at 182.9 nm are shown. The emission spectrum in figure 3 (*a*) was measured at the HIGITI set-up at 7 K and the spectrum in figure 3 (*b*) was obtained with the SPEX spectrofluorometer at room temperature. All emission lines can be assigned to *f–f* transitions. The emissions in figure 3 (*a*) are broad relative to the lines in figure 3 (*b*) due to the lower resolution of the VUV–UV emission monochromator at the HIGITI set-up. The majority of the emission lines in both spectra (those marked with •) correspond to transitions from the $^2F(2)_{7/2}$ state. The positions and the assignments are given in table 4, which shows that only a part of all $^2F(2)_{7/2}$ emissions that can be expected could be observed. The $^2F(2)_{7/2} \rightarrow ^2H(2)_{11/2}$ transition at 282 nm is clearly the most intense $^2F(2)_{7/2}$ emission. In the region 600–800 nm no emissions were observed at all, and thus it is not shown. Next to $^2F(2)_{7/2}$ transitions strong $^4S_{3/2}$, $^2H(2)_{11/2} \rightarrow ^4I_{15/2}$ emissions and weaker emissions from the $^2P_{3/2}$ level are present in figure 3 (*b*). The weak bands in figure 3 (*a*) at 228 and 244 nm can possibly be ascribed to the emissions from the $^2H(1)_{11/2}$ state at ~51 100 cm^{-1} to $^4I_{13/2}$ and $^4I_{11/2}$, respectively. These transitions were also observed in the emission spectrum upon $^2H(1)_{11/2}$ excitation (195.6 nm), albeit weak compared to the $^4D_{1/2}$ emissions. The occurrence of weak $^2H(1)_{11/2}$ emission is not unexpected since the gap to the next lower level is some 1900 cm^{-1} (table 2).

As the energy gap to the next lower $4f^{11}$ level is very large, emission could possibly occur from the $^2F(2)_{5/2}$ level around 63 300 cm^{-1}. However, for Er^{3+} in $LiYF_4$ the onset of the $4f^{10}5d$ configuration is at about 61 000 cm^{-1}, and the $4f^{11} \rightarrow 4f^{10}5d$ (f–d) absorption bands extend over a wide energy range [17]. To obtain emission from the $^2F(2)_{5/2}$ state the lowest $4f^{10}5d$ state should be at higher energy than the $^2F(2)_{5/2}$ level, otherwise non-radiative decay to the lowest $4f^{10}5d$ state is expected to be much more probable. In LaF_3 the lowest $4f^{n-1}5d$ level is at a very high energy for a lanthanide in a crystal. This is due to the ionic nature of the host and the large lanthanide site together with a high coordination number, which results in a small crystal-field splitting of the $5d$ states and thus a high energy of the lowest $4f^{n-1}5d$ state. It has been reported that the $4f^{10}5d$ onset for LaF_3:Er^{3+} is at a significantly higher position than for $LiYF_4$:Er^{3+} [24]. Therefore, the luminescence spectroscopy of LaF_3:Er^{3+} 1% was investigated.

In previous articles we have reported the existence of a $4f^{10}5d$ state with a higher spin quantum number ($2S+1=6$) than the $4f^{11}$ ground state ($2S+1=4$) [17]. This state (high-spin state) is at an energy just below the $4f^{10}5d$ states with the same spin quantum number as the ground state (low-spin states). For LaF_3:Er^{3+} the high-spin $4f^{10}5d$ state was observed around 66 000 cm^{-1} in the excitation spectrum, i.e. clearly higher in energy than the $^2F(2)_{5/2}$ level, which could not be observed in excitation. The VUV–UV and UV–visible emission spectra upon f–d excitation are presented in figures 4 (*a*) and (*b*), respectively. Many of the lines in these spectra are identified as emissions from the $^2F(2)_{5/2}$ state. As can be seen from table 4, in the VUV and UV spectral range all $^2F(2)_{5/2}$ emissions that can be expected are observed. At longer wavelengths a number of $^2F(2)_{5/2}$ emissions are obscured by other emissions such as $^4S_{3/2}$ and $^2P_{3/2}$ emissions, or are too weak to be observed. The strongest emission from the $^2F(2)_{5/2}$ level is the $^2F(2)_{5/2} \rightarrow {}^2H(2)_{9/2}$ transition at ~371 nm. The analogy with the strongest $^2F(2)_{7/2}$ emission ($^2F(2)_{7/2} \rightarrow {}^2H(2)_{11/2}$, see above) is striking: in both cases $\Delta S=0$, $\Delta L=+2$ and $\Delta J=+2$. Moreover, Nd^{3+} ($4f^3$) also has an emitting $^2F(2)_{5/2}$ level, from which the strongest emission is the $^2F(2)_{5/2} \rightarrow {}^2H(2)_{9/2}$ transition (~390 nm). Possibly, these transitions are hypersensitive transitions as they meet the criteria for hypersensitive transitions.

The $^2F(2)_{5/2} \rightarrow {}^4I_{15/2}$ emission is present as a shoulder on a strong and broad band at 161 nm, which is assigned to the transition from the high-spin $4f^{10}5d$ state to the ground state [17]. The f–d emission to the $^4I_{13/2}$ state is weakly observed at 180 nm. The observation that the f–d emission to the ground state lies at lower energy than the $^2F(2)_{5/2} \rightarrow {}^4I_{15/2}$ emission, although the $^2F(2)_{5/2}$ state is situated below the $4f^{10}5d$ states, is caused by the Stokes shift of the f–d emission. The situation is shown in the schematic configurational coordinate diagram in figure 5 (*a*). The parabolas were constructed using the experimental energies of the excitations and emissions. Only the $4f^{11}$ and $4f^{10}5d$ levels relevant for this discussion are shown. The excited vibrational levels of the electronic states have been omitted for clarity. From this diagram it can be understood that after non-radiative relaxation from the low-spin $4f^{10}5d$ state, emission from both the high-spin $4f^{10}5d$ state and the $^2F(2)_{5/2}$ levels can take place.

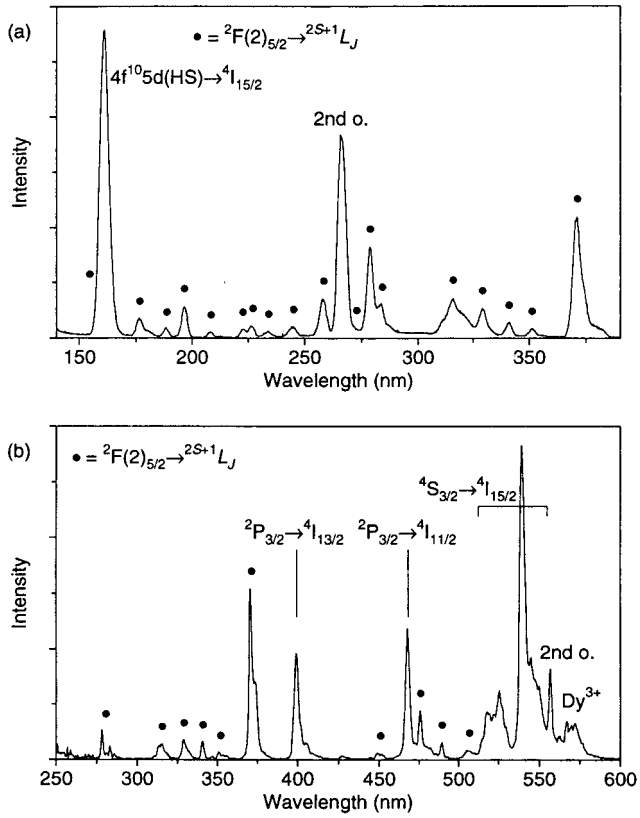

Figure 4. (*a*) VUV–UV emission spectrum of LaF_3:Er^{3+} 1% upon $^4I_{15/2} \rightarrow 4f^{10}5d$ excitation (133 nm) at 10 K. (*b*) UV–visible emission spectrum of LaF_3:Er^{3+} 1% upon $^4I_{15/2} \rightarrow 4f^{10}5d$ excitation (147 nm) at 300 K. For assignments of the $^2F(2)_{5/2}$ emissions (•) see table 4.

Next to $^2F(2)_{5/2}$ emission and f–d emission, in figure 4 (*a*) weak emission from the $^4D_{1/2}$ level is observed at 287, 314 and 380 nm. The strong peak at 266 nm is the second-order excitation and the f–d emission to the ground state is also present in second order around 320 nm. Finally, the weak emission around 470 and 570 nm in figure 4 (*b*) is due to a Dy^{3+} impurity.

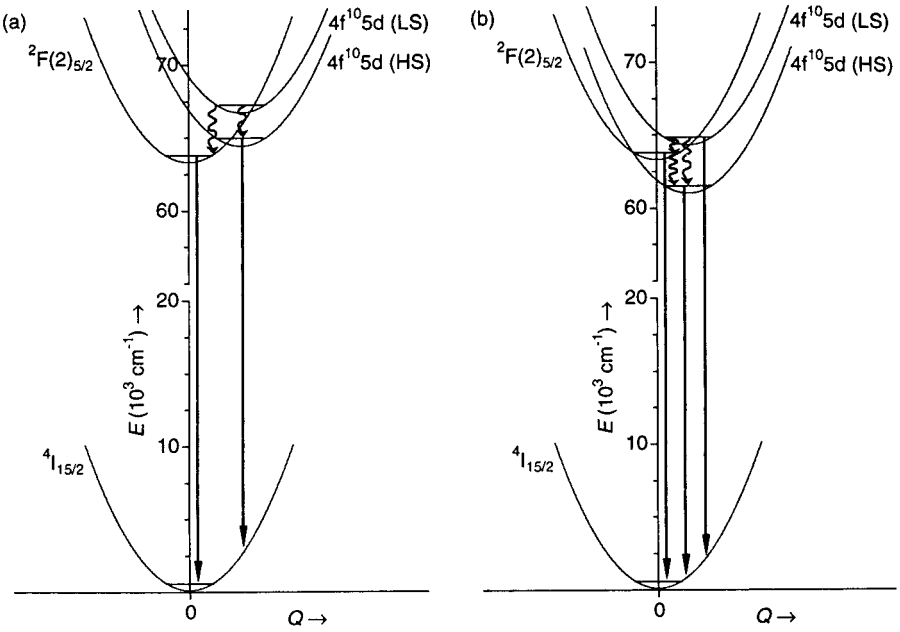

Figure 5. Schematic configurational coordinate diagrams for (*a*) Er^{3+} in LaF_3 and (*b*) Er^{3+} in $LiYF_4$ showing the decay processes upon excitation in the $4f^{10}5d$ states. Note the break in the energy scale.

Upon excitation in the low-spin $4f^{10}5d$ states of Er^{3+} in $LiYF_4$ efficient f–d emission occurs. Recently we have reported the occurrence of two types of f–d emission for $LiYF_4$:Er^{3+}: spin-forbidden emission from the high-spin (sextet) $4f^{10}5d$ state and spin-allowed emission from the lowest low-spin (quartet) state [17]. In addition to f–d emission, upon exciting in the low-spin $4f^{10}5d$ states we have observed weak emissions from the $^2F(2)_{5/2}$ state in the UV. The occurrence of $^2F(2)_{5/2}$ emission is unexpected, since for $LiYF_4$:Er^{3+} the $^2F(2)_{5/2}$ levels are situated in between the high-spin and the lowest low-spin $4f^{10}5d$ state, so that non-radiative decay to the high-spin state is expected to be efficient. However, the resemblance of the emission pattern (strong emission at 372 nm, weaker emissions at 280, 315, 331 and 342 nm) with that found for LaF_3:Er^{3+} and the absence of these emissions upon excitation in the high-spin $4f^{10}5d$ state or any other $4f^{11}$ state provide evidence that the assignment is correct. The configurational coordinate diagram in figure 5(*b*) illustrates the situation for $LiYF_4$:Er^{3+}. The occurrence of emission from the low-spin $4f^{10}5d$ state is explained by the fact that it is fully allowed and therefore fast so that it can compete with relaxation to the high-spin state, which is hindered as it requires one spin flip [17]. In contrast, emission from the $^2F(2)_{5/2}$ level is parity forbidden and thus relatively slow. To the best of our knowledge, intraconfigurational f–f emission from a $4f^n$ state situated at higher energies than the lowest-energetic $4f^{n-1}5d$ state has never been observed before. In this situation, which is also found for, e.g. Sm^{2+} and Eu^{2+} [25], fast relaxation to the lowest $4f^{n-1}5d$ state occurs and only f–d emission is observed. It is rather surprising that in the case of Er^{3+} in $LiYF_4$ emission from the $^2F(2)_{5/2}$ level can compete with relaxation to the high-spin $4f^{10}5d$ state, which is only some 2000 cm^{-1} lower in energy. To explain this observation we suggest the following: relaxation from the doublet $^2F(2)_{5/2}$ state to the sextet $4f^{10}5d$ state is inhibited by the spin selection rule because it requires two electron spins to change orientation. In addition, the ΔJ selection rule could also play a role. It has been shown before that the probability of non-radiative transitions within the $4f$ shell can be influenced by this rule [26]. Because of these selection rules, relaxation is slow and emission from the $^2F(2)_{5/2}$ level is observed, albeit weak.

From time-resolved measurements an estimate of the non-radiative relaxation rate to the high-spin state can be obtained. At room temperature the decay time of the $^2F(2)_{5/2}$ luminescence is about 0.2 μs, which is relatively short for a parity-forbidden f–f emission. For the luminescence decay of the spin-forbidden f–d emission a rise time of about 0.2 μs was found. This indicates that the high-spin $4f^{10}5d$ state is fed by non-radiative relaxation from the $^2F(2)_{5/2}$ level, which at the same time shortens the $^2F(2)_{5/2}$ lifetime. Since the intensity of the $^2F(2)_{5/2}$ emission is very low, the lifetime of the emission will be mainly due to non-radiative relaxation to the high-spin $4f^{10}5d$ state. As a result the $^2F(2)_{5/2}\rightarrow$ high-spin $4f^{10}5d$ relaxation rate is estimated to be about $5\times10^5\,s^{-1}$. At low temperature (10 K) the decay time of the $^2F(2)_{5/2}$ emission was too long to be determined with our appa-

ratus, but a rise time in the decay curve of the spin-forbidden *f–d* emission was present due to relaxation from the $^2F(2)_{5/2}$ level [17].

By examining the energies of various $^2F(2)_{5/2}$ emissions in $LiYF_4:Er^{3+}$ the position of the lowest $^2F(2)_{5/2}$ level was estimated to be around 63 300 cm^{-1} (table 2). A similar procedure resulted in the value of $\sim$47 200 cm^{-1} for $^4D_{1/2}$.

Finally, the luminescence of $YF_3:Er^{3+}$ 1% after *f–d* excitation was studied. The position of the $4f^{10}5d$ states for Er^{3+} in YF_3 is intermediate between those for Er^{3+} in LaF_3 and $LiYF_4$: the $^2F(2)_{5/2}$ state is at approximately the same energy as the high-spin $4f^{10}5d$ state. At 10 K $^2F(2)_{5/2}$ emission is observed in addition to spin-forbidden and spin-allowed *f–d* emission, just as for $LiYF_4:Er^{3+}$. At room-temperature emission from the $^2F(2)_{5/2}$ levels, as well as from the low-spin $4f^{10}5d$ state, has (nearly) vanished, indicating that relaxation to the high-spin state is much more efficient than at low temperature.

The $^2F(2)_{5/2}$ level is at slightly higher energy than the $^3P(1)_2$ level of Ho^{3+}, for which we have also reported emission [13]. As far as we are aware these levels are the highest-energy $4f^n$ levels from which emission has been reported so far for lanthanides. Based on the energy level schemes measured for these and other lanthanides in the VUV [12, 27], we do not expect that higher-lying emitting $4f^n$ levels will be found for lanthanides in solids.

In addition to resolving the high-energy levels of Er^{3+}, we are interested in the possibility of quantum cutting from one of these levels. It can be seen that on Er^{3+} sequential emission of two photons does occur: the $^4S_{3/2}$ and $^2P_{3/2}$ emissions in figures 3(*b*) and 4(*b*) follow on emissions from the high-energy levels to the $^4S_{3/2}$ and $^2P_{3/2}$ states, or levels just above, leading to population of these emitting states. In some cases both emissions are in the visible, e.g. the $^2F(2)_{7/2} \rightarrow {}^2P_{3/2}$ emission (433 nm) is followed by $^2P_{3/2} \rightarrow {}^4I_{11/2}$ (470 nm). For $^2F(2)_{5/2}$ as the starting level, there are even cascade processes yielding three visible photons: the various $^2F(2)_{5/2}$ emissions in the region 450–510 nm (table 4) are followed by multiphonon relaxation to the $^4D_{5/2}$ state, which leads to, for example, $^4D_{5/2} \rightarrow {}^4F_{9/2}$ emission at 428 nm and subsequently $^4F_{9/2} \rightarrow {}^4I_{15/2}$ emission around 650 nm (not shown in figure 4). Unfortunately, the visible quantum cutting processes do not take place with a high efficiency, since for all the high-lying emitting levels the strongest emissions lie in the UV. Therefore, it is concluded that a quantum efficiency in the visible higher than 100% can not be obtained for Er^{3+} alone, because losses in the UV (and IR) are always present. However, quantum cutting does occur and we have shown that it is possible to enhance the visible quantum efficiency by transfer of a part of the energy to Gd^{3+} [28]. Finally, it can be noted that the energy level scheme of Er^{3+} in LaF_3 may be interesting for obtaining a solid-state VUV laser: upon parity-allowed *f–d* excitation fast relaxation to a metastable $4f^{11}$ level occurs, from which VUV laser action can be expected.

4. Conclusions

An overview of the high-energy $4f^{11}$ levels of Er^{3+} in $LiYF_4$ is presented. A large number of the $4f^{11}$ levels expected in the region 39 000–65 000 cm^{-1} was observed in excitation spectra, and the energies were in good agreement with energy level calculations. Several high-lying emitting levels were identified, i.e. $^4D_{1/2}$ at $\sim$47 200 cm^{-1}, $^2F(2)_{7/2}$ at $\sim$54 700 cm^{-1} and $^2F(2)_{5/2}$ at $\sim$63 300 cm^{-1}. In $LaF_3:Er^{3+}$ the $^2F(2)_{5/2}$ state is situated just below the $4f^{10}5d$ states, so that upon *f–d* excitation $^2F(2)_{5/2}$ emission takes place efficiently. The occurrence of emission from the $^2F(2)_{5/2}$ level for Er^{3+} in $LiYF_4$ is remarkable as it lies just above the lowest $4f^{10}5d$ state. Probably this is due to slow relaxation from the $^2F(2)_{5/2}$ state to the sextet $4f^{10}5d$ state because of the spin-forbidden character of this non-radiative transition. As far as we are aware, the $^2F(2)_{5/2}$ level is the highest-energy $4f^n$ level from which emission can be obtained. Upon excitation in the high-lying levels of Er^{3+} quantum cutting occurs, but an efficient quantum cutter in the visible region based on Er^{3+} alone is not possible.

References

[1] Ronda, C. R., 1995, *J. Alloys Compounds*, **225,** 534.
[2] Sommerdijk, J. L., Bril, A., and de Jager, A. W., 1974, *J. Lumin.*, **8,** 341.
[3] Piper, W. W., DeLuca, J. A., and Ham, F. S., 1974, *J. Lumin.,* **8,** 344.
[4] Pappalardo, R., 1976, *J. Lumin.*, **14,** 159.
[5] Nieuwesteeg, K. J. B. M., 1989, *Philips J. Res.*, **44,** 383.
[6] Dieke, G. H., 1968, *Spectra and Energy Levels of Rare Earth Ions in Crystals* (New York: Interscience Publishers).
[7] Carnall, W. T., Goodman, G. L., Rajnak, K., and Rana, R. S., 1988, A Systematic Analysis of the Spectra of the Lanthanides Doped into Single Crystal LaF_3 (Argonne, IL: Argonne National Laboratory).
[8] Khaidukov, N. M., Kirikova, N. Y., Krupa, J. C., Makhov, V. N., Negodin, E., and Zimmerer, G., 2002, *Proc. SPIE Int. Soc. opt. Eng.*, **4766,** 154.
[9] Vlasenko, A. A., Devyatkova, L. I., Ivanova, O. N., Mikhailin, V. V., Chernov, S. P., Uvarova, T. V., and Sobolev, B. P., 1985, *Sov. Phys. Dokl.*, **30,** 395.
[10] Devyatkova, L. I., Ivanova, O. N., Mikhailin, V. V., Rudnev, S. N., and Chernov, S. P., 1987, *Opt. Spectrosc.* (USSR), **62,** 275.
[11] Devyatkova, K. M., Ivanova, O. N., Seiranyan, K. B., Tamazyan, S. A., and Chernov, S. P., 1990, *Sov. Phys. Dokl.*, **35,** 40.

[12] Wegh, R. T., Donker, H., Meijerink, A., Lamminmäki, R. J., and Hölsä, J., 1997, *Phys. Rev.* B, **56,** 13 841.
[13] Peijzel, P. S., Wegh, R. T., Meijerink, A., Hölsä, J. H., and Lamminm, R. J., 2002, *Opt. Commun.*, **204,** 195.
[14] Wegh, R. T., Donker, H., Oskam, K. D., and Meijerink, A., 1999, *Science,* **283,** 663; Wegh, R. T., Donker, H., Oskam, K. D., and Meijerink, A., 1999, *J. Lumin.*, **82,** 93.
[15] Riseberg, L. A., and Weber, M. J., 1976, *Progress in Optics XIV*, edited by E. Wolf (Amsterdam: North-Holland), p. 116.
[16] Robinson, M., 1986, *J. cryst. Growth*, **75,** 184.
[17] Wegh, R. T., and Meijerink, A., 1999, *Phys. Rev.* B, **60,** 10 820.
[18] Brown, M. R., Roots, K. G., and Shand, W. A., 1969, *J. Phys. C solid state Phys.*, **2,** 593.
[19] Couto dos Santos, M. A., Antic-Fidancev, E., Gesland, J. Y., Krupa, J. C., Lemaître-Blaise, M., and Porcher, P., 1998, *J. Alloys Compounds*, **275–277,** 435.
[20] Ellens, A., Schenker, S., Meijerink, A., and Blasse, G., 1996, *J. Lumin.*, **69,** 1.
[21] Burdick, G. W., and Richardson, F. S., 1998, *Chem. Phys.*, **228,** 81.
[22] Miller, S. A., Rast, H. E., and Caspers, H. H., 1970, *J. chem. Phys.*, **52,** 4172.
[23] von Lips, H., Schwentner, N., Sliwinski, G., and Petermann, K., 1995, *J. appl. Spectrosc.*, **62,** 803.
[24] Yang, K. H., and DeLuca, J. A., 1978, *Phys. Rev.* B, **17,** 4246.
[25] Dujardin, C., Moine, B., and Pedrini, C., 1993, *J. Lumin.*, **54,** 259.
[26] Riseberg, L. A., and Weber, M. J., 1976, *Progress in Optics XIV*, edited by E. Wolf (Amsterdam: North-Holland).
[27] Wegh, R. T., Meijerink, A., Lamminmäki, R. J., and Hölsä, J., 2000, *J. Lumin.*, **87–89,** 1002.
[28] Wegh, R. T., van Loef, E. V. D., and Meijerink, A., 2000, *J. Lumin.*, **90,** 111.